BCSJ

BF_3-Functionalized Silica-Coated Magnetic Nanoparticles as a Novel Heterogeneous Solid Acid for Synthesis of Formazan Derivatives via a Green Protocol

Abdolhamid Bamoniri* **and Naimeh Moshtael-Arani**

Department of Organic Chemistry, Faculty of Chemistry, University of Kashan, Kashan, Iran

E-mail: bamoniri@kashanu.ac.ir

Received: October 6, 2014; Accepted: January 15, 2015; Web Released: January 22, 2015

A new type of green heterogeneous solid acid was prepared by the immobilization of $BF_3 \cdot Et_2O$ on the surface of $Fe_3O_4@SiO_2$ core–shell nanocomposite ($Fe_3O_4@SiO_2$–BF_3) and characterized by Fourier transform infrared spectroscopy (FT-IR), X-ray diffraction (XRD), vibrating sample magnetometer (VSM), field emission scanning electron microscope (FE-SEM), energy-dispersive X-ray (EDS), and transmission electron microscope (TEM). The activity of this super solid acid was probed through the synthesis of aryl diazonium salts as the starting reactant and then, their diazo coupling with aldehyde phenylhydrazones for formation of formazan derivatives in a solvent-free medium at room temperature. This clean and environmentally benign methodology has advantages such as: no need for corrosive and toxic liquid acids, solvents, or buffer solutions, room temperature reaction, high yields, and short reaction times. In addition, long-term stability of aryl diazonium salts supported on the surface of $Fe_3O_4@SiO_2$–BF_3 magnetic nanoparticles (MNPs) at room temperature was one of the most important results of this procedure.

At the beginning of the new century, synthesis of organic compounds under solvent-free conditions has received much attention,[1–5] as it provides manipulative simplicity, greater selectivity, easier workup, shorter reaction times and higher yields which matches with the green chemistry protocol. Formazans are colored compounds due to their π–π^* electronic transitions and form a distinct class of organic dyes with certain properties. These compounds have received much attention for their applications in analytical chemistry,[6] biological applications,[7] and as dyestuffs.[8] Their antiviral,[9] antimicrobial,[10] anti-inflammatory, analgesic,[11] antifungal,[12] anticancer, anti-HIV,[13] photo- and thermochromic activities[14] are also of utmost importance. Although so far a lot has been known about numerous synthesized formazans and their structural, spectral features and reaction mechanisms of their formation,[15–25] their difficult synthetic conditions including the control of temperature between 0–5 °C and medium pH between 10–12, and problems such as time-consuming preparation of buffer solutions with specific concentrations, incompatibility with the environment due to the use of toxic liquid acids and solvents, instability of aryl diazonium salts at room temperature, and finally the long reaction times and modest yields, have prevented formazans from gaining widespread use in industry. Accordingly, the development of novel and simple methods for solving the above mentioned problems and efficient synthesis of formazans is an interesting challenge. Nowadays, solid acids have resolved most of these drawbacks and improved activity and selectivity rather than individual reagents.[26–30] In this regard, nanostructure solid acids exhibit higher activity and selectivity than their corresponding bulk materials due to their large surface to volume ratio.[31–33] Recently, silica-coated MNPs[34] have emerged as a new kind of efficient catalyst support because of advantages such as biocompatibility, hydrophilicity, low toxicity, high surface area, and ease of surface modification with various organic and inorganic materials to achieve certain purposes especially in the field of catalysis.[35–42] Motivated by the special properties of $Fe_3O_4@SiO_2$ nanoparticles and high acidity of $BF_3 \cdot SiO_2$, and in continuation of our efforts on the development of efficient solid acids for useful synthetic organic transformations[43–47] herein we report the preparation and characterization of a novel and eco-friendly magnetic solid acid as $Fe_3O_4@SiO_2$–BF_3 and its utility for the synthesis of formazan dyes in a solvent-free environment at room temperature. To the best of our knowledge, this research is the first report about long-term stability of aryl diazonium salts supported on the surface of MNPs and their use as the reactant for synthesis of formazans in solvent-free conditions. The findings of this research may have implications for an effective synthesis on a larger scale in dyeing and medical industries.

Results and Discussion

This research was performed in two stages. Initially, $Fe_3O_4@SiO_2$–BF_3 MNPs were synthesized and identified by FT-IR, XRD, VSM, FE-SEM, EDS, and TEM techniques. In the second stage, formazan derivatives were synthesized by solvent-free mixing aryl diazonium salts supported on MNPs and aldehyde phenylhydrazones at room temperature.

Synthesis and Characterization of $Fe_3O_4@SiO_2$–BF_3 Nanoparticles. $Fe_3O_4@SiO_2$–BF_3 core–shell nanoparticles, with Fe_3O_4 spheres as the core and silica-supported BF_3 as the shell, were prepared by a simple, low cost, and convenient method. At first, Fe_3O_4 nanoparticles were prepared by the coprecipitation of $FeCl_2$ and $FeCl_3$ in ammonia solution. To improve the chemical stability of Fe_3O_4, its surface engineering

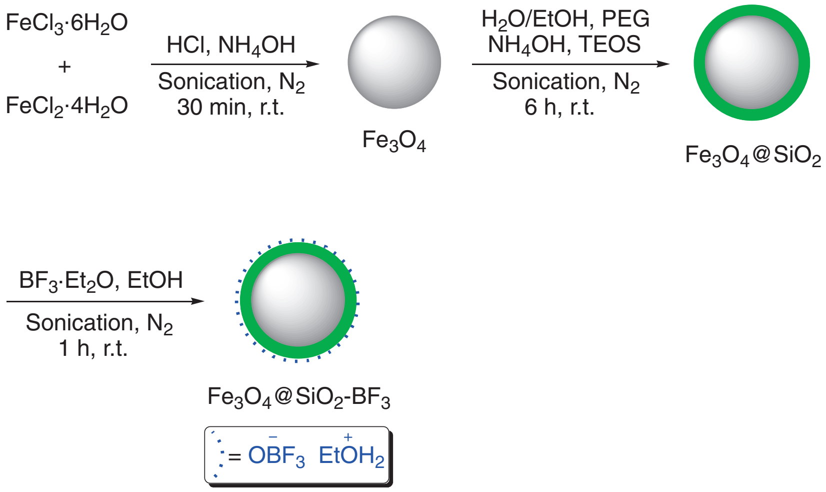

Scheme 1. The schematic diagram for synthesis of $Fe_3O_4@SiO_2$–BF_3 MNPs.

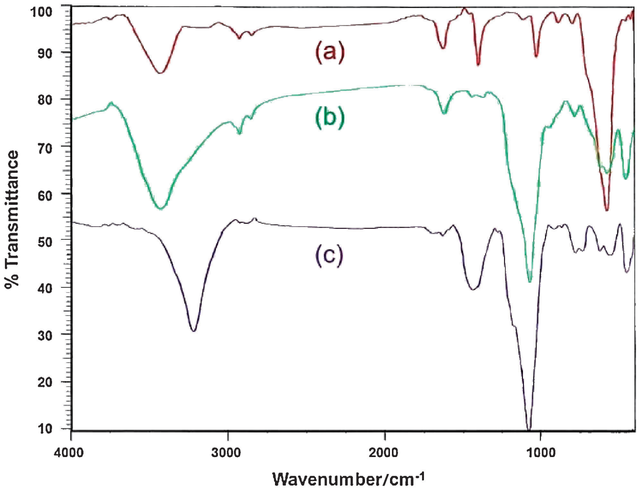

Figure 1. FT-IR spectra of a) Fe_3O_4, (b) $Fe_3O_4@SiO_2$, and (c) $Fe_3O_4@SiO_2$–BF_3.

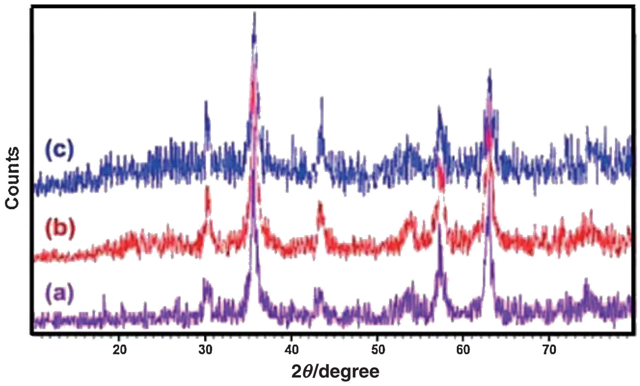

Figure 2. XRD patterns of (a) Fe_3O_4, (b) $Fe_3O_4@SiO_2$, and (c) $Fe_3O_4@SiO_2$–BF_3.

was successfully performed by the suitable deposition of SiO_2 onto Fe_3O_4 surface via the ammonia-catalyzed hydrolysis of tetraethyl orthosilicate (TEOS). Next, the $Fe_3O_4@SiO_2$ spheres served as support for the immobilization of BF_3 groups by simple stirring of $Fe_3O_4@SiO_2$ and $BF_3·Et_2O$ in ethanol. All three steps were carried out under sonication (Scheme 1).

In order to identify the molecular structures of Fe_3O_4, $Fe_3O_4@SiO_2$, and $Fe_3O_4@SiO_2$–BF_3 MNPs, FT-IR analysis of three mentioned samples was performed (Figure 1). Fe_3O_4 was identified by a stretching vibration of the Fe–O absorption peak at 576 cm^{-1}, O–H stretching vibration at 3429 cm^{-1}, and O–H deformed vibration at 1625 cm^{-1} in Figure 1a. The FT-IR spectrum of $Fe_3O_4@SiO_2$ (Figure 1b) displayed characteristic peaks at 1093 and 800 cm^{-1} corresponding to symmetrical and asymmetrical vibrations of Si–O–Si, respectively. The weak band at 466 cm^{-1} corresponded to the Si–O–Fe stretching vibrations of the $Fe_3O_4@SiO_2$ core–shell, overall confirming the presence of SiO_2 in the sample. The successful covalent linking of the $BF_3·Et_2O$ on the surface of $Fe_3O_4@SiO_2$ core–shell was proved by the appearance of a new band at 1457 cm^{-1}, which originates from the absorption of B–O (Figure 1c). The absorption band of B–F was hidden under the Si–O band. Also, the ethanolic OH and existing moisture in $BF_3·Et_2O$ caused a broad O–H stretching band at a wavenumber of 3221 cm^{-1}. Again observation of Fe_3O_4 absorption peaks in Figures 1b and 1c implies that Fe_3O_4 MNPs do not change chemically or physically after coating and surface modification processes. According to this information and regarding the reported structure of $BF_3·SiO_2$ in the literature,[48] the final structure of nano $Fe_3O_4@SiO_2$–BF_3 was predicted (Scheme 1).

Figure 2 shows the XRD powder diffraction patterns of three synthesized MNPs. The data for the Fe_3O_4 nanoparticles at 2θ of 30.22, 35.61, 43.25, 53.58, 57.30, 62.89, and 74.66° (Figure 2a) corresponded to the standard Fe_3O_4 powder diffraction data. Moreover, the relatively sharp peaks observed indicate phase purity of Fe_3O_4 nanoparticles, which are consistent with the presence of the cubic inverse spinel structure of Fe_3O_4. The XRD pattern of the $Fe_3O_4@SiO_2$ (Figure 2b) was in good agreement with that of Fe_3O_4 phase, except for a broad peak around 2θ of 20–30° corresponding to amorphous phase of SiO_2. This indicates that the MNPs obtained after the coating process are composed of Fe_3O_4 core and amorphous SiO_2 shell. The XRD pattern of the modified $Fe_3O_4@SiO_2$ with $BF_3·Et_2O$ in Figure 2c was nearly the same as Figure 2b, which it seems that the surface modification by BF_3 groups has little effect

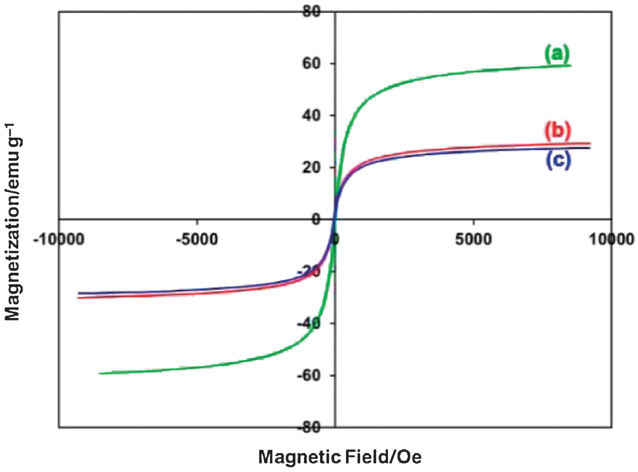

Figure 3. Magnetization curves of (a) Fe_3O_4, (b) $Fe_3O_4@SiO_2$, and (c) $Fe_3O_4@SiO_2–BF_3$.

on the XRD pattern of $Fe_3O_4@SiO_2$ nanoconpmosite, because of the shielding effect of Fe_3O_4 and SiO_2 peaks. However, decrease in the signal to noise ratio in Figure 2c compared to Figure 2b can verify the linking of BF_3 on the surface of $Fe_3O_4@SiO_2$ core–shell MNPs. Furthermore, characteristic peaks of Fe_3O_4 were observed in three samples, thereby indicating that the binding process did not induce any phase change.

The magnetic properties of synthesized Fe_3O_4, $Fe_3O_4@SiO_2$, and $Fe_3O_4@SiO_2–BF_3$ nanoparticles were assessed by VSM at room temperature. The magnetization curve in Figure 3 indicates magnetization as a function of applied magnetic field. The saturation magnetization of the $Fe_3O_4@SiO_2$ nanocomposite was about 29.15 emu g^{-1} (Figure 3b), and this reduced to 27.44 emu g^{-1} after supporting with $BF_3{\cdot}Et_2O$ (Figure 3c). Both of these values were much lower than the initial saturation magnetization of Fe_3O_4 nanoparticles (59.2 emu g^{-1}) in Figure 3a. The decrease of the saturation magnetization after surface coating of Fe_3O_4 confirms the presence of a diamagnetic outer shell (SiO_2 or $SiO_2–BF_3$) at the surface of the Fe_3O_4 particles.

The high-magnification FE-SEM images of the purified MNPs are displayed in Figures 4a–4c. These images clearly showed the surface morphology of three kinds of synthesized MNPs with a nearly spherical shape. Elemental components of three MNPs were characterized by EDS analysis. Figure 4d shows EDS of the Fe_3O_4 nanoparticles, in which the particles contain Fe and O elements. The presence of Fe, O, and Si elements in Figure 4e verified the coating of Fe_3O_4 core by SiO_2 shell. The appearance of two new signals related to F and C elements in Figure 4f confirmed supporting of $BF_3{\cdot}Et_2O$ on $Fe_3O_4@SiO_2$ core–shell nanoparticles according to the final structure of $Fe_3O_4@SiO_2–BF_3$ presented in Scheme 1.

TEM images of Fe_3O_4 and $Fe_3O_4@SiO_2–BF_3$ together with their size distribution histograms are displayed in Figure 5. As demonstrated in Figure 5a, Fe_3O_4 nanoparticles have the spherical morphology. In Figure 5b, two regions with different electron densities can be distinguished that confirms the Fe_3O_4 nanoparticles were successfully coated with a thin layer of a different phase. However, it can be observed that the sample is nearly in core–shell structure. An electron dense region (black colour) which corresponds to Fe_3O_4 cores and a less dense or more translucent region (ash colour) surrounding these cores that is $SiO_2–BF_3$ shell. About 100 nanoparticles were considered for each sample to obtain their size distribution histograms. From the size distribution histograms, the average size of 9 nm for Fe_3O_4 and 13 nm for $Fe_3O_4@SiO_2–BF_3$ nanoparticles could be estimated.

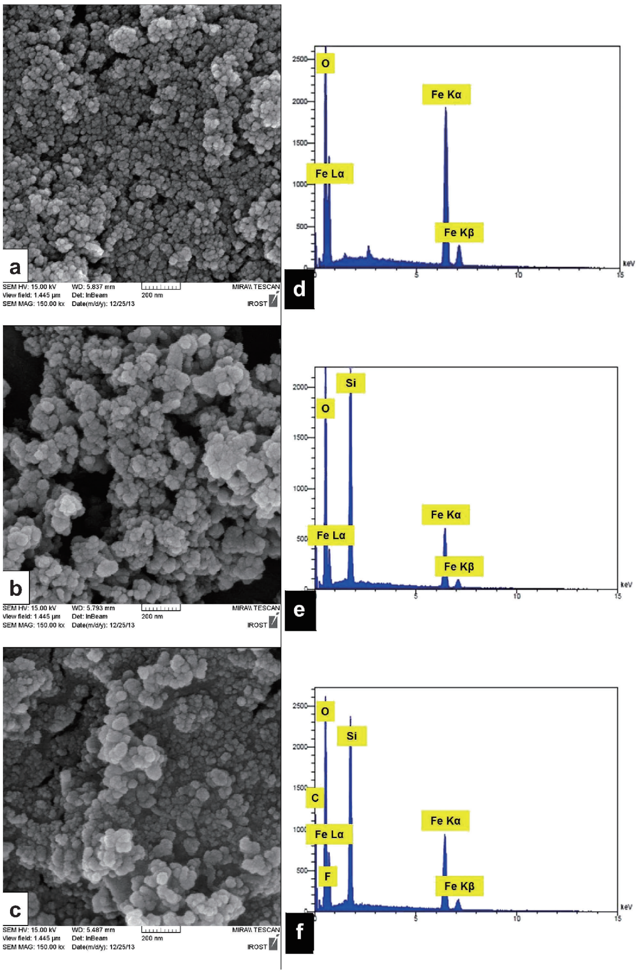

Figure 4. FE-SEM images of (a) Fe_3O_4, (b) $Fe_3O_4@SiO_2$, (c) $Fe_3O_4@SiO_2–BF_3$ and EDS spectra of (d) Fe_3O_4, (e) $Fe_3O_4@SiO_2$, (f) $Fe_3O_4@SiO_2–BF_3$.

Finally, $Fe_3O_4@SiO_2–BF_3$ was identified by using the techniques described above, and applied for synthesis of formazan derivatives.

Synthesis and Characterization of Formazan Derivatives 3a–3q. The most common synthetic route to the formazan compounds **3a–3q** involves coupling of aryl diazonium salts **1a–1g** with aldehyde phenylhydrazones **2a–2i** in a basic medium. As synthesis of formazans is a highly time-consuming reaction with modest yields, which requires special conditions such as low temperature, using buffer solutions to adjust pH and liquid acids to synthesize diazonium salts,[15–25] we tried to solve all these problems by the development a green and facile procedure for synthesis of formazans.

At first, the efficiency of $Fe_3O_4@SiO_2–BF_3$ MNPs in diazotization reaction, followed by diazo coupling with alde-

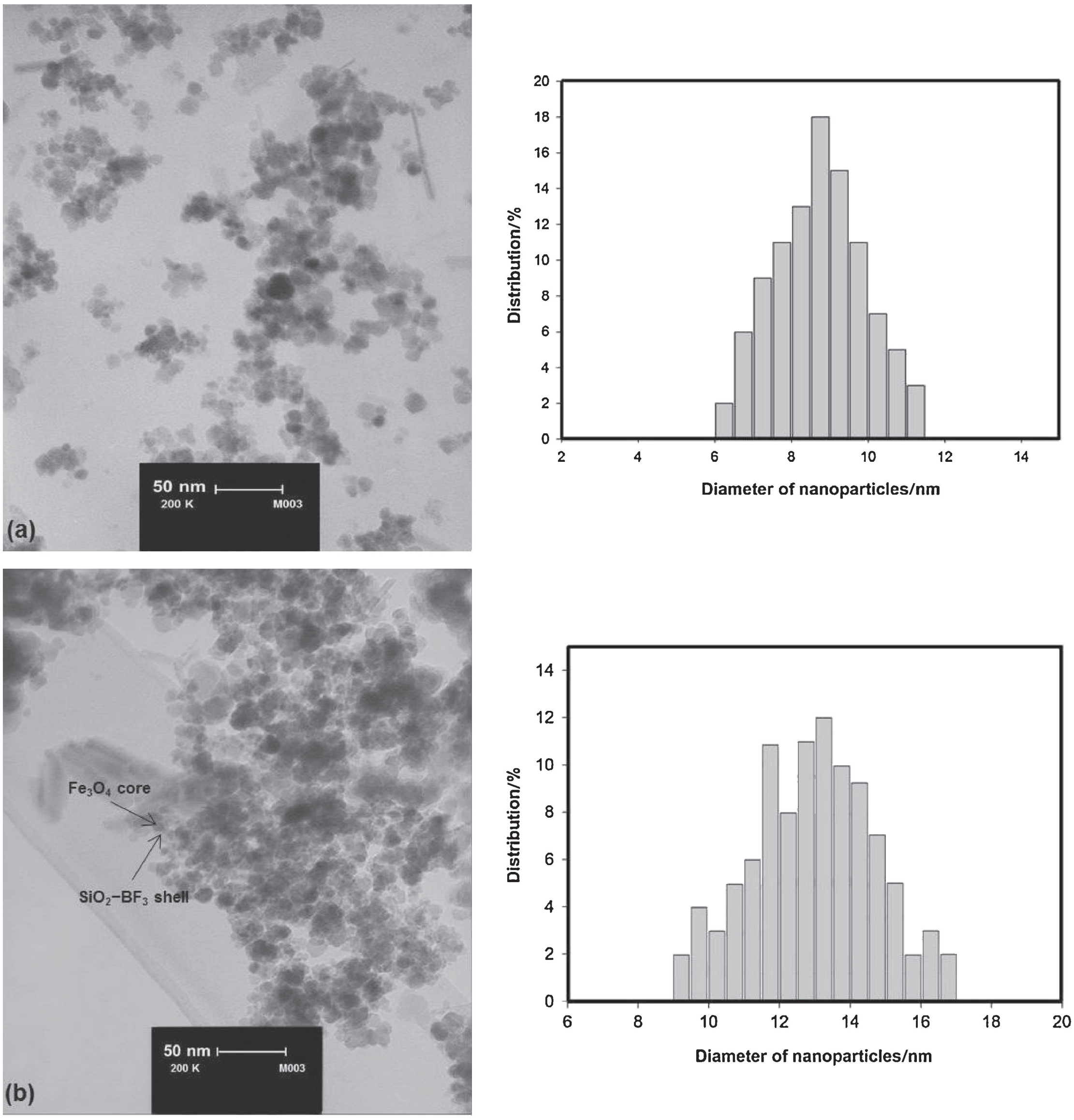

Figure 5. TEM images of (a) Fe_3O_4 and (b) $Fe_3O_4@SiO_2$–BF_3 nanoparticles along with size distribution histograms.

hyde phenylhydrazones, was explored via a model reaction. 4-Chloroaniline was selected as a model substrate and screened for a range of parameters such as effect of various acids, stability of 4-chlorophenyl diazonium salt (**1d**) at room temperature, time of diazotization, and yield of resulted formazan (**3h**). The observed results are summarized in Table 1.

According to Table 1, the mild and protic solid acids such as silica phosphoric acid and silica chloride gave the corresponding formazan (**3h**) with modest yields of 43% and 48%, respectively (Table 1, Entries 1 and 2). The stability of 4-chlorophenyl diazonium salt (**1d**) supported on the above mentioned acids was at maximum 2 days. Lewis acids such as Fe_3O_4, $Fe_3O_4@SiO_2$, and $BF_3{\cdot}Et_2O$ sources were also tested individually. There was no reaction in the presence of Fe_3O_4, $Fe_3O_4@SiO_2$, and $BF_3{\cdot}Et_2O$ (Table 1, Entries 3–5), while the yield of formazan **3h** in the presence of $BF_3{\cdot}SiO_2$ (Table 1, Entry 6) as a strong protic acid was obtained 63%. These results clearly indicated that the presence of Brønsted acid sites on the solid acid surface is an essential factor for promoting diazotization reaction. In other words, diazotization only occurs in the presence of Brønsted acids. One of the interesting points of using $BF_3{\cdot}SiO_2$, in addition to decrease the reaction time, was the long-term stability of aryl diazonium salt (**1d**) supported on the surface of this solid acid compared to silica phosphoric acid and silica chloride. So, $BF_3{\cdot}SiO_2$ showed better performance than the other above mentioned acids (Table 1, Entries 1–5). In order to improve the yield of reaction, we decided to prepare a protic solid acid with similar properties to $BF_3{\cdot}SiO_2$ in stabilizing aryl diazonium salts and reducing the reaction time. So, $Fe_3O_4@SiO_2$–BF_3 nanoparticles as a novel protic solid acid was synthesized and its performance tested in diazotization reaction. $Fe_3O_4@SiO_2$–BF_3 nanoparticles with different loadings afforded the improved yield of 79% to 87% for formazan **3h** (Table 1, Entries 7–10).

In another comparative study (Table 1, Entries 7–10), the effect of $Fe_3O_4@SiO_2$ loading by $BF_3{\cdot}Et_2O$ on the acidic performance of $Fe_3O_4@SiO_2$–BF_3 was investigated. Although the time of diazotization and the stability of 4-chlorophenyl diazo-

Table 1. Comparison of Efficiency of Various Acids for Synthesis of Formazan (**3h**)

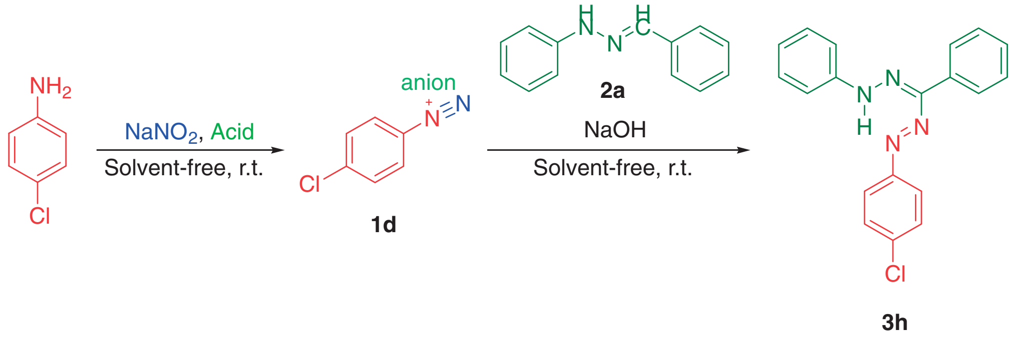

Entry	Acid (wt %)	Stability at r.t.	Time of diazotization	Yield$^{a)}$/%
1	Silica phosphoric acid (10)	$\sim$2 days	35 min	43
2	Silica chloride (10)	$\sim$2 days	30 min	48
3	Fe_3O_4	—	No reaction	—
4	$Fe_3O_4@SiO_2$	—	No reaction	—
5	$BF_3 \cdot Et_2O$	—	No reaction	—
6	$BF_3 \cdot SiO_2$ (10)	$>$12 months	1 min	63
7	$Fe_3O_4@SiO_2–BF_3$ (5)	$>$12 months	12 s	79
8	$Fe_3O_4@SiO_2–BF_3$ (10)	$>$12 months	6 s	87
9	$Fe_3O_4@SiO_2–BF_3$ (15)	$>$12 months	8 s	83
10	$Fe_3O_4@SiO_2–BF_3$ (20)	$>$12 months	8 s	80

a) The yields refer to the isolated pure formazan (**3h**) after adding fresh 4-chlorophenyl diazonium salt (**1d**) into basic benzaldehyde phenylhydrazone (**2a**).

nium salt (**1d**) supported on $Fe_3O_4@SiO_2–BF_3$ nanoparticles with different loadings in the same conditions were approximately identical, but 10 wt % $Fe_3O_4@SiO_2–BF_3$ resulted in the highest yield of formazan **3h** (Table 1, Entry 8). In conclusion, 10 wt % $Fe_3O_4@SiO_2–BF_3$ was selected as the most ideal solid acid for synthesis of formazans **3a–3q** among those listed in Table 1.

As previously mentioned, with more investigations, it was found that 4-chlorophenyl diazonium salts (**1d**) supported on $Fe_3O_4@SiO_2–BF_3$ nanoparticles underwent no significant change at room temperature for several months. In order to prove this case, we prepared large amounts of 4-chlorophenyl diazonium salt (**1d**) and kept it at room temperature without any special conditions to test at different times. Then, diazo coupling of this diazonium salt (**1d**) with benzaldehyde phenylhydrazone (**2a**) was repeated every month under the same conditions and the yield of formazan (**3h**) measured. The results presented in Figure 6 indicate that the yield of formazan (**3h**) changes from 87% to 80% after 12 months from preparation time of diazonium salt (**1d**).

To explore the reason for aryl diazonium salt stability (**1d**), its FT-IR spectrum was studied (Figure 7). In this spectrum, the ethanolic OH and existing moisture in $BF_3 \cdot Et_2O$ caused a broad O–H stretching band at a wavenumber of 3419 cm^{-1}. The appearance of a new band at 2289 cm^{-1} clearly demonstrated N≡N stretching vibration and verified the formation of diazonium salt (**1d**). The absorption bands of B–O and Si–O vibrations were observed at 1442 and 1085 cm^{-1}, respectively. Aromatic C–H bending vibrations, C–Cl and Fe–O stretching bands were revealed at 829, 634, and 586 cm^{-1}, respectively.

According to this information, the structure of aryl diazonium salts **1a–1g** supported on MNPs was surmised. Scheme 2 reveals that in this probable structure, aryl diazonium cations are located on the surface of negatively charged particles called Fe_3O_4–silica triflouroborate anions. So, the presence of bulky anions and charge–charge interactions between nitrogen and boron atoms are the possible reasons for the unusual stability of these salts.

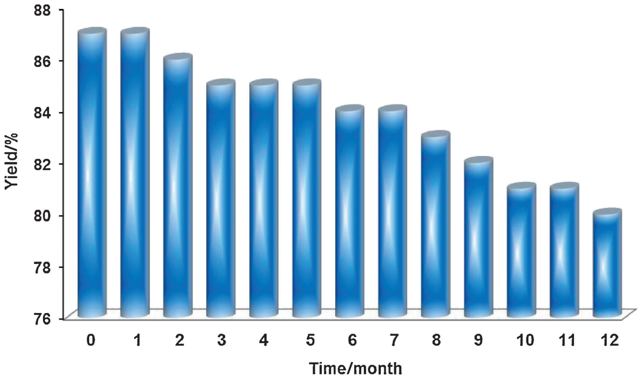

Figure 6. The yield of formazan **3h** prepared from the stable 4-chlorophenyl diazonium salt (**1d**) at different times.

As a result, the excellent conversions of aniline derivatives to aryl diazonium salts **1a–1g** and their long-term stability showed that the $Fe_3O_4@SiO_2–BF_3$ has strong and sufficient protic sites, which are responsible for its excellent performance in synthesis of formazan derivatives **3a–3q**.

Diazo coupling of aldehyde phenylhydrazones **2a–2i** with aryl diazonium salts **1a–1g** in basic medium was the final step of formazan dyes **3a–3q** formation. According to Scheme 3, for full conversion of intermediate to formazan, medium pH should be changed from 7 to 10–12. In order to control and fixate the medium pH, different buffer solutions have been used in the literature,[17,18,21–25] while in our research by using grinding procedure in the absence of solvent, there is no need to use buffer solution for pH adjustment. Hence, one of the significant results of our methodology compared to previous methods, there was no requirement for buffering solution to adjust medium pH.

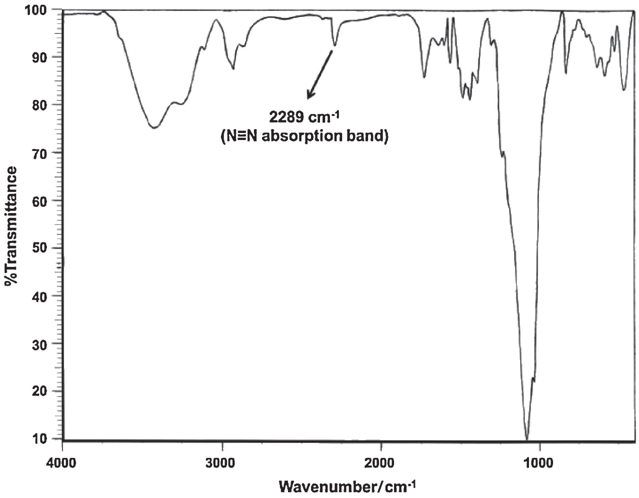

Figure 7. FT-IR spectrum of 4-chlorophenyl diazonium salt (**1d**) supported on Fe_3O_4@SiO_2–BF_3 MNPs.

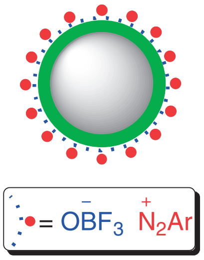

Scheme 2. The probable structure of aryl diazonium salt **1a**–**1g** supported on Fe_3O_4@SiO_2–BF_3 nanoparticles.

Formazans are usually synthesized around 0–5 °C, because temperatures above 5 °C cause decomposition of diazonium salts and conversion to side products before coupling with aldehyde phenylhydrazones.[15–25] This is the main reason for the relatively low yield of formazans. To overcome this limitation, we decided to use Fe_3O_4@SiO_2–BF_3 MNPs as a solid acid to be able to do the reaction at room temperature. In conclusion, the stability of aryl diazonium salts supported on Fe_3O_4@SiO_2–BF_3, significantly increased the efficiency of formazans synthesis. Final results of reaction times and yields were clarified in Table 2.

It is important to note that Fe_3O_4@SiO_2–BF_3 in diazotization reaction acts as a two-function reagent, so that not only its acidic protons convert the nitrite anions (NO_2^-) in $NaNO_2$ to nitrosonium cations (NO^+) to promote diazotization, but also its bulky anions cause the stability of aryl diazonium cations.

In total, we hope that Fe_3O_4@SiO_2–BF_3 as an environmentally benign inherent solid acid catalyst, in addition to the application for the synthesis of formazans, would have a promising potential for many industrially important catalytic processes.

Conclusion

A green and highly effective methodology for the synthesis of formazan derivatives **3a**–**3q** was developed by solvent-free diazo coupling of aryl diazonium salts **1a**–**1g** with basic aldehyde phenylhydrazones **2a**–**2i** at room temperature. Using Fe_3O_4@SiO_2–BF_3 as a novel heterogeneous super solid acid in the diazotization step and solvent-free procedure provided experimental simplicity, compatibility with the environment, no use of special conditions such as buffer solution and low

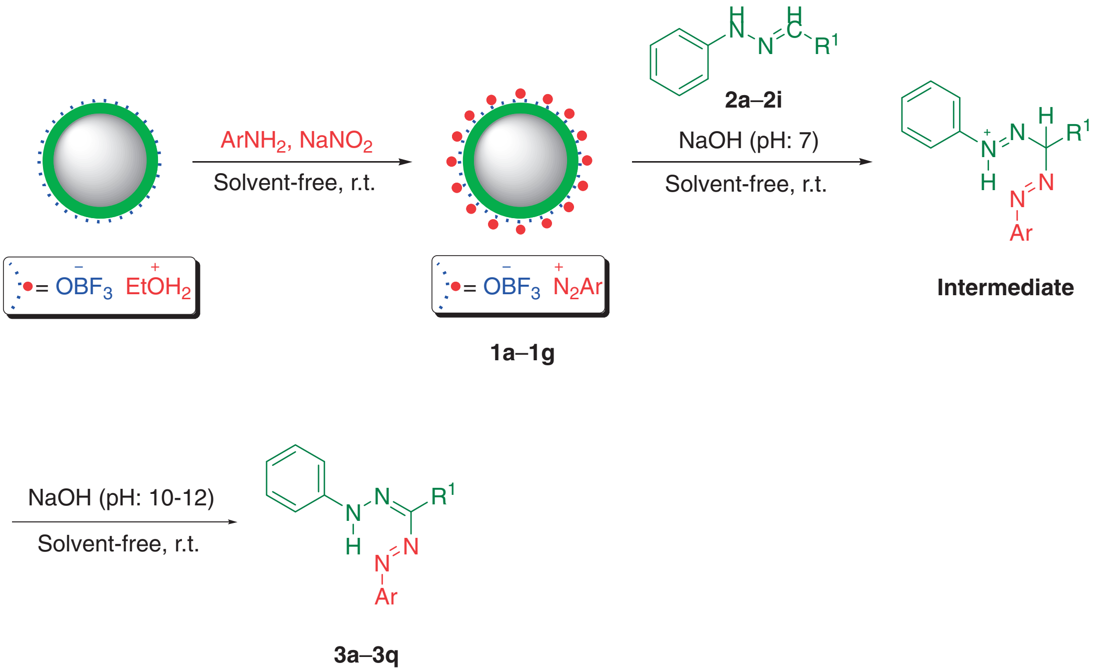

Scheme 3. Synthesis of formazans **3a**–**3q** in the presence of Fe_3O_4@SiO_2–BF_3 under solvent-free condition.

Table 2. Diazo Coupling of Aryl Diazonium Salts **1a**–**1g** with Aldehyde Phenylhydrazones **2a**–**2i** for Synthesis of Formazans **3a**–**3q** under Solvent-Free Condition

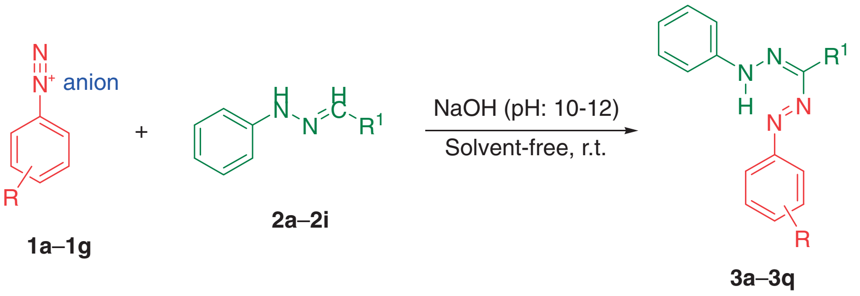

Entry	Diazonium salt	Aldehyde phenylhydrazone	Formazan	Yield[a)]/%
1	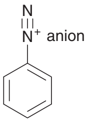 **1a**	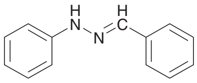 **2a**	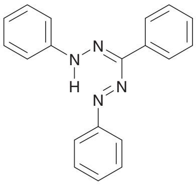 **3a**	86
2	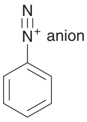 **1a**	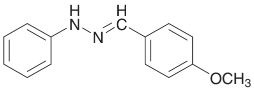 **2b**	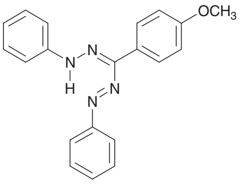 **3b**	88
3	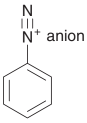 **1a**	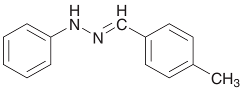 **2c**	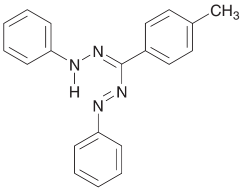 **3c**	87
4	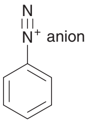 **1a**	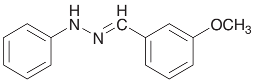 **2d**	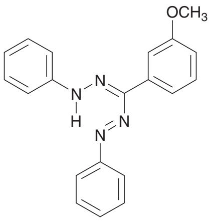 **3d**	84
5	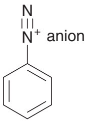 **1a**	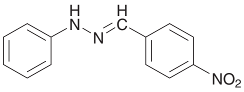 **2e**	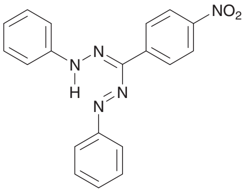 **3e**	85

Continued on next page.

Continued.

Entry	Diazonium salt	Aldehyde phenylhydrazone	Formazan	Yield[a]/%
6	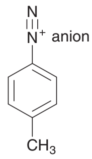 **1b**	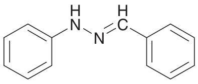 **2a**	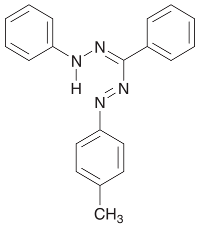 **3f**	89
7	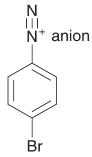 **1c**	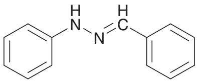 **2a**	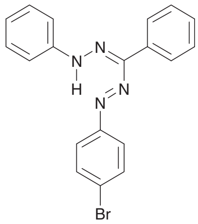 **3g**	86
8	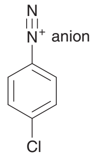 **1d**	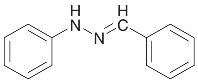 **2a**	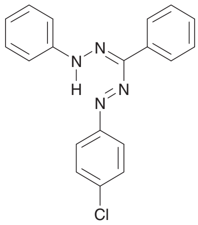 **3h**	87
9	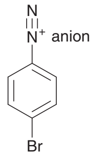 **1c**	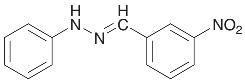 **2f**	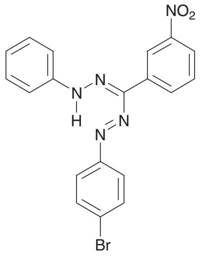 **3i**	90
10	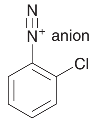 **1e**	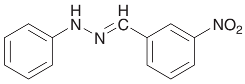 **2f**	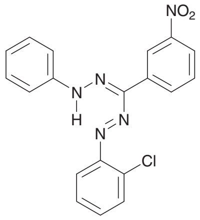 **3j**	82

Continued on next page.

Continued.

Entry	Diazonium salt	Aldehyde phenylhydrazone	Formazan	Yield[a)]/%
11	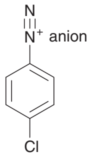 **1d**	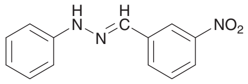 **2f**	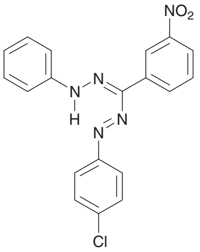 **3k**	84
12	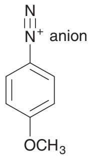 **1f**	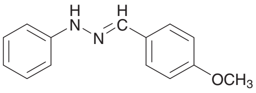 **2b**	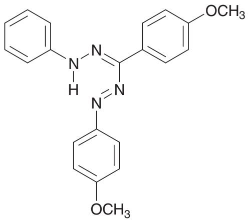 **3l**	92
13	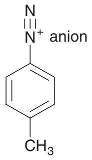 **1b**	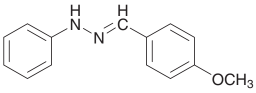 **2b**	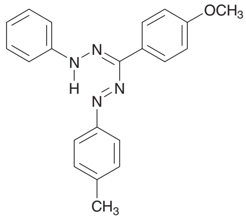 **3m**	88
14	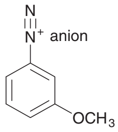 **1g**	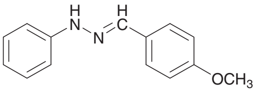 **2b**	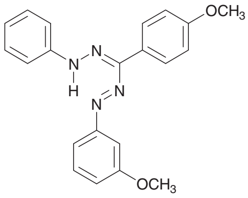 **3n**	91
15	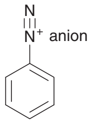 **1a**	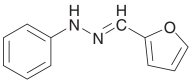 **2g**	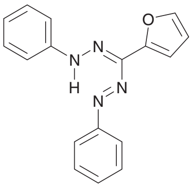 **3o**	89
16	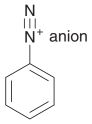 **1a**	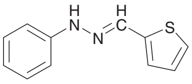 **2h**	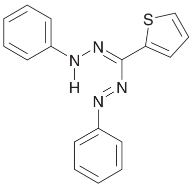 **3p**	87

Continued on next page.

Continued.

Entry	Diazonium salt	Aldehyde phenylhydrazone	Formazan	Yield[a)]/%
17	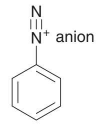 **1a**	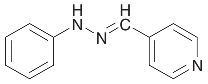 **2i**	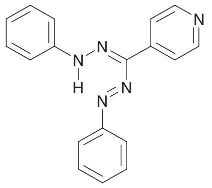 **3q**	90

a) Overall isolated yield after purification.

temperature, efficient yields, short reaction times and made this procedure attractive to synthesize a variety of these compounds. The structure and stability of aryl diazonium salts **1a**–**1g** supported on Fe_3O_4@SiO_2–BF_3 MNPs were studied, too.

Experimental

Materials and Apparatus. Chemicals and solvents were purchased from Merck and Sigma-Aldrich Companies. Melting points were obtained with a micro melting point apparatus (Electrothermal, Mk3) and are uncorrected. UV–vis (Ultraviolet–visible) spectra were taken with a double beam Perkin-Elmer 550S spectrophotometer in the range of 200–600 nm, using spectrophotometric grade ethanol as the blank. FT-IR spectra were run on a Nicolet Magna 550 spectrometer. ^{1}H NMR spectra were recorded on a Bruker DRX-400 Avance spectrometer. Tetramethylsilane (TMS) was used as an internal reference and deuterated chloroform used as solvent. The ultrasonic equipment used for the synthesis of MNPs (Fe_3O_4, Fe_3O_4@SiO_2, and Fe_3O_4@SiO_2–BF_3) was a *Sonica 2200ETH S3 SOLTEC* ultrasonic bath (Italy) with a working frequency of 40 KHz. XRD patterns were acquired using a Philips Xpert MPD diffractometer equipped with a Cu Kα anode ($\lambda = 1.54$ Å) in the 2θ range from 10 to 80°. Magnetization of the samples was recorded as a function of the applied magnetic field sweeping between ±10 kOe at room temperature. All measurements were performed on a vibrating sample magnetometer device (Meghnatis Daghigh Kavir Co., Kashan Kavir, Iran). The morphology of the synthesized samples was studied with a Mira II LMU Tescan FE-SEM made in Czech Republic. Elemental composition of three above-mentioned MNPs was investigated by EDS spectroscopy (SAMX, France). Fe_3O_4 and Fe_3O_4@SiO_2–BF_3 average size and distribution were analyzed by TEM using a Philips CM120 with a LaB6 cathode and accelerating voltage of 120 kV.

Synthesis of Fe_3O_4@SiO_2–BF_3 MNPs. The synthesis of Fe_3O_4 nanoparticles was carried out according to a known procedure using chemical coprecipitation by a little modification of methodology already reported in the literature.[49] Briefly, $FeCl_3 \cdot 6H_2O$ (8.0 g, 0.029 mol) and $FeCl_2 \cdot 4H_2O$ (3.5 g, 0.017 mol) with a molar ratio of approximately 2:1, were dissolved in 38 mL of deoxygenated 0.4 M HCl solution. Then, 375 mL of deoxygenated 0.7 M ammonia solution was quickly added into the reaction mixture under sonication and nitrogen atmosphere. This resulted in immediate formation of a black precipitate of Fe_3O_4 (magnetite). The sonication of magnetite dispersion was continued for 30 min. Finally, the precipitates were collected using an external magnetic field and washed several times with distilled water and ethanol. The synthesized Fe_3O_4 MNPs were suspended in 50 mL of distilled water for use in the next steps.

Modified Stöber sol–gel process[50] was used for coating magnetite nanoparticles with a silica shell. Typically, 50 mL of magnetite suspended in water was added to 250 mL ethanol and sonicated at room temperature for 20 min under nitrogen flow. Then 11.85 mL PEG 200, 50 mL of distilled water, 25 mL NH_3 (28%) were added respectively, and after 15 min, 5 mL of TEOS was introduced into the suspension and the mixture was again sonicated for 6 h. Fe_3O_4@SiO_2 nanocomposite was centrifuged at 3000 rpm for 10 min, the solvent was discarded and nanoparticles were washed three times with water and then ethanol and dried in vacuum at room temperature.

In the final stage, $BF_3 \cdot Et_2O$ (0.45 mL) was added dropwise to a slurry containing Fe_3O_4@SiO_2 core–shell nanoparticles (4.5 g) and ethanol (15 mL). The mixture was sonicated for 1 h at room temperature. The resulting suspension was filtered and dried at room temperature to obtain a brown solid named nano Fe_3O_4@SiO_2–BF_3 (10 wt %). The acidic capacity of Fe_3O_4@SiO_2–BF_3 nanoparticles was 0.72 mmol g^{-1} and determined via titration of 0.5 g of solid acid with standard solution of NaOH.

Typical Procedure for the Synthesis of Formazan Derivatives 3a–3q. In order to synthesize aryl diazonium salts **1a**–**1g**, aromatic amines (2 mmol) were ground with $NaNO_2$ (3 mmol) and 10 wt % Fe_3O_4@SiO_2–BF_3 (0.3 g) in a mortar with a pestle. Then, synthesized aryl diazonium salt **1a**–**1g** was added to a ground mixture of aldehyde phenylhydrazone **2a**–**2i** and NaOH (necessary amount to reach pH of 10–12 after diazo coupling). Upon mixing two reactants in basic medium, the color of the mixture changed to red. Anyway, the mixture was ground at room temperature for 1–2 min. After completion of the reaction (TLC), the mixture was washed with distilled water (50 mL) and then acetone (30 mL). Evaporation of the solvent followed by flash column chromatography (in the case of compounds **3d**, **3e**, **3j**, washing by hot ethanol was performed instead of flash column chromatography) that gave formazans in high yields. The structures of formazans **3a**–**3q** were characterized by spectroscopic methods such as UV–vis, FT-IR, and ^{1}H NMR.

The authors are grateful to University of Kashan for supporting this work by Grant No. 159189/40.

Supporting Information

Supporting Information including spectroscopic data for final products in Table 2 is available electronically on J-STAGE.

References

1 B. M. Smith, T. M. Kubczyk, A. E. Graham, *Tetrahedron* **2012**, *68*, 7775.

2 S. Koley, S. Chowdhury, T. Chanda, B. J. Ramulu, M. S. Singh, *Tetrahedron* **2013**, *69*, 8013.

3 Z. Wei, J. Li, N. Wang, Q. Zhang, D. Shi, K. Sun, *Tetrahedron* **2014**, *70*, 1395.

4 S. Muthusaravanan, C. Sasikumar, B. D. Bala, S. Perumal, *Green Chem.* **2014**, *16*, 1297.

5 A. B. Atar, Y. S. Jeong, Y. T. Jeong, *Tetrahedron* **2014**, *70*, 5207.

6 B. N. Barsoum, S. K. Khella, A. H. M. Elwaby, A. A. Abbas, Y. A. Ibrahim, *Talanta* **1998**, *47*, 1215.

7 G. Mariappan, R. Korim, N. M. Joshi, F. Alam, R. Hazarika, D. Kumar, T. Uriah, *J. Adv. Pharm. Technol. Res.* **2010**, *1*, 396.

8 Z. Yuzhen, L. Dongzhi, *Dyes Pigm.* **1995**, *29*, 57.

9 D. D. Mukerjee, S. K. Shukla, B. L. Chowdhary, *Arch. Pharm. (Weinheim, Ger.)* **1981**, *314*, 991.

10 A. B. Samel, N. R. Pai, *J. Chem. Pharm. Res.* **2010**, *2*, (4), 60.

11 R. Kalsi, K. Pande, T. N. Bhalla, S. S. Parmar, J. P. Barthwal, *Pharmacology* **1988**, *37*, 218.

12 K. G. Desai, K. R. Desai, *J. Heterocycl. Chem.* **2006**, *43*, 1083.

13 S. D. Bhardwaj, V. S. Jolly, *Asian J. Chem.* **1997**, *9*, 48.

14 G. I. Sigeikin, G. N. Lipunova, I. G. Pervova, *Russ. Chem. Rev.* **2006**, *75*, 885.

15 H. J. Cottrell, D. L. Pain, R. Slack, *J. Chem. Soc.* **1954**, 2968.

16 A. A. Katritzky, S. A. Belyakov, D. Cheng, H. D. Durst, *Synthesis* **1995**, 577.

17 H. Tezcan, Ş. Can, R. Tezcan, *Dyes Pigm.* **2002**, *52*, 121.

18 H. Tezcan, N. Ozkan, *Dyes Pigm.* **2003**, *56*, 159.

19 N. A. Frolova, S. Z. Vatsadze, N. Yu. Vetokhina, V. E. Zavodnik, N. V. Zyk, *Mendeleev Commun.* **2006**, *16*, 251.

20 N. A. Frolova, S. Z. Vatsadze, A. I. Stash, R. D. Rakhimov, N. V. Zyk, *Chem. Heterocycl. Compd.* **2006**, *42*, 1444.

21 H. Tezcan, E. Uzluk, *Dyes Pigm.* **2007**, *75*, 633.

22 H. Tezcan, E. Uzluk, M. L. Aksu, *J. Electroanal. Chem.* **2008**, *619–620*, 105.

23 H. Tezcan, G. Ekmekci, *Acta Chim. Slov.* **2010**, *57*, 189.

24 H. Tezcan, N. Tokay, *Spectrochim. Acta, Part A* **2010**, *75*, 54.

25 H. Tezcan, H. Şenöz, N. Tokay, *Monatsh. Chem.* **2012**, *143*, 579.

26 B. Datta, M. A. Pasha, *Ultrason. Sonochem.* **2013**, *20*, 303.

27 F. Jing, B. Katryniok, E. Bordes-Richard, S. Paul, *Catal. Today* **2013**, *203*, 32.

28 Y.-B. Huang, Y. Fu, *Green Chem.* **2013**, *15*, 1095.

29 K. M. Hello, H. R. Hasan, M. H. Sauodi, P. Morgen, *Appl. Catal., A* **2014**, *475*, 226.

30 J. G. Hernández-Cortez, M. Manríquez, L. Lartundo-Rojas, E. López-Salinas, *Catal. Today* **2014**, *220–222*, 32.

31 E. Rafiee, M. Khodayari, M. Kahrizi, R. Tayebee, *J. Mol. Catal. A: Chem.* **2012**, *358*, 121.

32 S. M. Inamdar, V. K. More, S. K. Mandal, *Tetrahedron Lett.* **2013**, *54*, 579.

33 A. Landarani Isfahani, I. Mohammadpoor-Baltork, V. Mirkhani, M. Moghadam, A. R. Khosropour, S. Tangestaninejad, M. Nasr-Esfahani, H. Amiri Rudbari, *Synlett* **2014**, *25*, 645.

34 M. Gao, W. Li, J. Dong, Z. Zhang, B. Yang, *World J. Condens. Matter Phys.* **2011**, *1*, 49.

35 Y.-H. Liu, J. Deng, J.-W. Gao, Z.-H. Zhang, *Adv. Synth. Catal.* **2012**, *354*, 441.

36 X. Zhang, X. He, L. Chen, Y. Zhang, *J. Mater. Chem.* **2012**, *22*, 16520.

37 H.-J. Xu, X. Wan, Y.-Y. Shen, S. Xu, Y.-S. Feng, *Org. Lett.* **2012**, *14*, 1210.

38 G. M. Ucoski, F. S. Nunes, G. DeFreitas-Silva, Y. M. Idemori, S. Nakagaki, *Appl. Catal., A* **2013**, *459*, 121.

39 S. Wang, Z. Zhang, B. Liu, J. Li, *Catal. Sci. Technol.* **2013**, *3*, 2104.

40 M. R. Nabid, Y. Bide, M. Niknezhad, *ChemCatChem* **2014**, *6*, 538.

41 F. Zhang, M. Chen, X. Wu, W. Wang, H. Li, *J. Mater. Chem. A* **2014**, *2*, 484.

42 M. Shakourian-Fard, A. H. Rezayan, S. Kheirjou, A. Bayat, M. M. Hashemi, *Bull. Chem. Soc. Jpn.* **2014**, *87*, 982.

43 B. F. Mirjalili, A. Bamoniri, A. Akbari, *J. Iran. Chem. Soc.* **2011**, *8*, S135.

44 A. Bamoniri, A. Ghorbani-Choghamarani, B. F. Mirjalili, *Phosphorus, Sulfur Silicon Relat. Elem.* **2011**, *186*, 381.

45 B. F. Mirjalili, A. Bamoniri, L. Zamani, *Sci. Iran.* **2012**, *19*, 565.

46 B. F. Mirjalili, A. Bamoniri, M. A. Mirhoseini, *Chem. Heterocycl. Compd.* **2012**, *48*, 856.

47 A. Bamoniri, B. F. Mirjalili, S. Nazemian, *J. Iran. Chem. Soc.* **2014**, *11*, 653.

48 K. Wilson, J. H. Clark, *Chem. Commun.* **1998**, 2135.

49 M. Emadi, E. Shams, M. K. Amini, *J. Chem.* **2013**, 787682.

50 W. Stöber, A. Fink, E. Bohn, *J. Colloid Interface Sci.* **1968**, *26*, 62.